NeuroImage 79 (2013) 72–80

Contents lists available at SciVerse ScienceDirect

NeuroImage

journal homepage: www.elsevier.com/locate/ynimg

Quantification of opioid receptor availability following spontaneous epileptic seizures: Correction of [^{11}C]diprenorphine PET data for the partial-volume effect

Colm J. McGinnity [a,b,c], Miho Shidahara [d], Maria Feldmann [e,f], Shiva Keihaninejad [g], Daniela A. Riaño Barros [a,b], Ioannis S. Gousias [a,b], John S. Duncan [e,f], David J. Brooks [a], Rolf A. Heckemann [a,b,h], Federico E. Turkheimer [a,b,i], Alexander Hammers [a,b,e,f,h,*], Matthias J. Koepp [e,f]

[a] Centre for Neuroscience, Department of Medicine, Imperial College London, London W12 0NN, UK
[b] Medical Research Council Clinical Sciences Centre, London W12 0NN, UK
[c] Department of Clinical Neuroscience, Institute of Psychiatry, King's College London, London SE5 8AF, UK
[d] Division of Medical Physics, Tohoku University Graduate School of Medicine, Sendai, Japan
[e] Department of Clinical and Experimental Epilepsy, Institute of Neurology, University College London, London WC1N 3BG, UK
[f] Epilepsy Society, Chalfont St. Peter, Buckinghamshire SL9 0RJ, UK
[g] Department of Neurodegenerative Diseases, Institute of Neurology, University College London, London WC1N 3BG, UK
[h] The Neurodis Foundation, CERMEP Imagerie du Vivant, 69003 Lyon, France
[i] Centre for Neuroimaging Sciences, Institute of Psychiatry, King's College London, London SE5 8AF, UK

ARTICLE INFO

Article history:
Accepted 5 April 2013
Available online 15 April 2013

Keywords:
Temporal lobe epilepsy
Opioids
PET
Diprenorphine
Partial-volume
Hippocampus

ABSTRACT

Previous positron emission tomography (PET) studies in refractory temporal lobe epilepsy (TLE) using the non-selective opioid receptor antagonist [^{11}C]diprenorphine (DPN) did not detect any changes in mesial temporal structures, despite known involvement of the hippocampus in seizure generation. Normal binding in smaller hippocampi is suggestive of increased receptor concentration in the remaining grey matter. Correction for partial-volume effect (PVE) has not been used in previous DPN PET studies. Here, we present PVE-corrected DPN-PET data quantifying post-ictal and interictal opioid receptor availability in humans with mTLE.

Eight paired datasets of post-ictal and interictal DPN PET scans and eleven test/retest control datasets were available from a previously published study on opioid receptor changes in TLE following seizures (Hammers et al., 2007a). Five of the eight participants with TLE had documented hippocampal sclerosis. Data were re-analyzed using regions of interest and a novel PVE correction method (structural functional synergistic-resolution recovery (SFS-RR); (Shidahara et al., 2012)). Data were denoised, followed by application of SFS-RR, with anatomical information derived via precise anatomical segmentation of the participants' MRI (MAPER; (Heckemann et al., 2010)). [^{11}C]diprenorphine volume-of-distribution (V_T) was quantified in six regions of interest.

Post-ictal increases were observed in the ipsilateral fusiform gyri and lateral temporal pole. A novel finding was a post-ictal increase in [^{11}C]DPN V_T relative to the interictal state in the ipsilateral parahippocampal gyrus, not observed in uncorrected datasets. As for voxel-based (SPM) analyses, correction for global V_T values was essential in order to demonstrate focal post-ictal increases in [^{11}C]DPN V_T.

This study provides further direct human *in vivo* evidence for changes in opioid receptor availability in TLE following seizures, including changes that were not evident without PVE correction. Denoising, resolution recovery and precise anatomical segmentation can extract valuable information from PET studies that would be missed with conventional post-processing procedures.

© 2013 Published by Elsevier Inc.

Introduction

The opioid peptide receptor (OPR) system comprises μ (MOP), δ (DOP), κ (KOP) and nociceptin/orphanin FQ (NOP; also known as ORL-1) opioid peptide receptors (for review: (Dhawan et al., 1996; Satoh and Minami, 1995)), which bind endogenous opioids known as enkephalins and endorphins. The receptors are coupled to G-protein, and have seven transmembrane domains (Chaturvedi et al., 2000).

Abbreviations: [^{11}C]DPN, [^{11}C]diprenorphine; DOP, δ opioid peptide; KOP, κ opioid peptide; HS, hippocampal sclerosis; MAPER, multi-atlas propagation using enhanced registration; MOP, μ-opioid peptide; MR, magnetic resonance; OPR, opioid peptide receptor; PVE, partial volume effect; SFS-RR, structural functional synergistic-resolution recovery; TLE, temporal lobe epilepsy; V_T, volume-of-distribution.

* Corresponding author at: Neurodis Foundation, CERMEP — Imagerie du Vivant, Hôpital Neurologique Pierre Wertheimer, 59 Boulevard Pinel, 69003 Lyon, France. Fax: +33 4 72 68 86 10.
E-mail address: alexander.hammers@fondation-neurodis.org (A. Hammers).

1053-8119/$ – see front matter © 2013 Published by Elsevier Inc.
http://dx.doi.org/10.1016/j.neuroimage.2013.04.015

There is growing evidence for an anticonvulsant action of these endogenous peptides, in a 'tonic antiepileptic' system that is hypothesized to limit the spread of electrical activity within the temporal lobe (Hammers et al., 2007a; Koepp and Duncan, 2000; Mayberg et al., 1991). The most convincing evidence implies a role for opioid peptides in post-ictal seizure inhibition (Engel et al., 1981; Pirker et al., 2009). It remains difficult to ascribe this to a single opioid receptor subtype; recent work in prodynorphin knockouts implicates the kappa receptor (Loacker et al., 2007), whereas activation of the mu-opioid receptor has a 'bi-directional' influence (for review: (Tortella, 1988)).

PET studies of opioid-receptor mediated neurotransmission in epilepsy have provided evidence for a dynamic relationship between opioid peptide receptor availability and seizures (for review: (Hammers and Lingford-Hughes, 2006)). Interictal studies suggest increased MOP and DOP receptor availability in the ipsilateral temporal lobe during the interictal period in temporal lobe epilepsy (TLE; (Frost et al., 1988; Madar et al., 1997; Mayberg et al., 1991)). Ictal studies of reading-induced and absence epilepsies suggest decreased opioid MOP-, DOP- and KOP-receptor availability during seizures (Bartenstein et al., 1993; Koepp et al., 1998). Post-ictal opioid peptide receptor availability is increased in the ipsilateral temporal lobe in TLE (Hammers et al., 2007a).

All PET studies to date have failed to demonstrate or explicitly document significant alteration of hippocampal or parahippocampal gyrus opioid peptide receptor binding (interictal or post-ictal) in TLE (for review (Hammers and Lingford-Hughes, 2006)). This is surprising, given the association of these regions with TLE. The finding of apparently normal opioid peptide receptor availability in sclerotic hippocampi suggests that the opioid binding per neuron is actually upregulated in these regions. Recently, increased hippocampal mu-opioid receptor mRNA expression and G-protein binding was documented in humans with refractory TLE *ex vivo* (Cuellar-Herrera et al., 2012). It should be noted that radioligands such as [^{11}C] diprenorphine are not subtype-selective, and so density alterations of the different subtypes in opposing directions could cancel each other out when ligand binding is being measured. However, the possibility that failure to detect hippocampal or parahippocampal alterations is the result of the limited resolution of the PET system and associated partial-volume effect (PVE) has not been assessed.

The PVE consists of the blurring of focal PET activity distribution by a 'point-spread function' due to suboptimal camera resolution with consequential signal 'spill out' into surrounding regions. A consequence of this 'intensity diffusion' is the under- and over-estimation of regional concentrations of radioactivity (Aston et al., 2002; Meltzer et al., 1996).

Intensity diffusion is of particular relevance to studies of temporal lobe epilepsy. Regions of interest such as the hippocampi, parahippocampal gyri, and amygdalae are small structures. This problem is exacerbated by the volume loss of mesial temporal sclerosis that is frequently observed in TLE, an effect that is not limited to the hippocampi, and may be bilateral. For example, gliosis and neuronal loss in the amygdala ('amygdala sclerosis') has been reported in isolation and also in 35–76% of patients with hippocampal sclerosis (HS) at post-mortem ((ILAE Commission on Neurosurgery of Epilepsy, 2004; Yilmazer-Hanke et al., 2000)). Volume loss in the parahippocampal gyrus is also recognized (Bernasconi et al., 2003). The accuracy of quantification of the activity from such regions is therefore decreased, as the activity from anatomically smaller regions is underestimated in a non-linear fashion (Hoffman et al., 1979).

'Structural functional synergistic-resolution recovery' (SFS-RR; (Shidahara et al., 2009, 2012)) is a novel partial-volume effect correction method that has been evaluated in simulations and in human [^{18}F]FDG and [^{11}C]raclopride PET studies. The model is flexible in that the reliance upon structural data is varied relative to the quality of anatomical detail (for example, MRI data is weighted more strongly than CT data). The method uses the wavelet transform (WT) (Mallat, 1989; Turkheimer et al., 1999) to decompose the functional images (such as PET) and structural reference image (such as MRI) into several resolution elements. The high-resolution component of the PET image is then replaced with the scaled structural image, based on the assumption that the conventional PET image does not have enough high-resolution components. To suppress distribution mismatch between functional and anatomical images, an individualized frequency based atlas (Hammers et al., 2003) was used as the structural reference image in the validation studies. The authors demonstrated that the use of such an atlas outperforms the use of CT/MRI data alone (Shidahara et al., 2009).

Here we describe the application of SFS-RR, enhanced with more accurate automated as well as manual region definitions, to the data acquired by (Hammers et al., 2007a,b) for the accurate quantification of [^{11}C]DPN binding in regions vulnerable to intensity diffusion. Our objective was to accurately quantify post-ictal and interictal opioid receptor binding in participants with refractory TLE, in order to correlate clinical variables with the correctly quantified opioid binding per unit of grey matter.

Our primary hypothesis was that decreased interictal [^{11}C]DPN V_T would be evident in the sclerotic hippocampus of participants whose TLE is associated with HS. Our secondary hypothesis was that increased post-ictal [^{11}C]DPN V_T would also be evident in mesial temporal structures, in addition to our previous finding of post-ictal increases in [^{11}C]DPN V_T in the extra-mesial ipsilateral temporal lobe in PVE-uncorrected data.

Material and methods

The datasets for this study had been previously acquired for another study, which did not use PVE correction. Details of participants' demographics and clinical data, PET and other data acquisition have been described in detail elsewhere (Hammers et al., 2007a,b). Briefly, for re-analysis eight participants with refractory TLE (four males; median age 45.5 years, range 32–60 years) who were scanned interictally, and also post-ictally within 22 h (median 10.0 h, range 1.5–21.3 h) after spontaneous temporal lobe seizures were available. The diagnosis of TLE was based on history, seizure semiology, interictal EEG features and neuropsychological examination. The lateralization of TLE was additionally based on MRI findings and ictal EEG (when available; seven of eight participants, including all 'MRI-normal' participants). One of the original nine participants with refractory TLE (number 5) was excluded from re-analysis due to irretrievable loss of MRI data. Eleven healthy controls (eight males; median age 42.0 years, range 30–58 years) had been scanned twice under the same conditions.

PET data acquisition and analysis

Images had been acquired using a Siemens/CTI ECAT EXACT3D 966 PET camera over 90 min, subsequent to injection of a median dose of 185 MBq (range 130–200 MBq) of [^{11}C]DPN. 3D Volumetric T1-weighted MRI scans were acquired for co-registration with the PET dataset using a 1.0 T Picker HPQ scanner (Robert Steiner MRI unit, Hammersmith Hospital; voxel sizes 1 mm × 1 mm × 1.3 mm) or a 1.5 T General Electric Signa Echospeed scanner (National Society for Epilepsy; voxel sizes 0.9375 mm × 0.9375 mm × 1.5 mm).

Derivation of individual arterial plasma input functions corrected for metabolism has been described elsewhere (Hammers et al., 2007a,b). Briefly, continuous (first 15 min) and discrete arterial blood sampling was used to determine the partition of radioactivity and the parent fraction (Luthra et al., 1993).

Dynamic images, metabolite-corrected arterial plasma input functions (COMIF; in-house software), and spectral analysis (Cunningham and Jones, 1993) implemented in RPM (Turkheimer et al., 2003) (Gunn et al., internal software), were used to create voxel-by-voxel parametric images of [^{11}C]DPN volume-of-distribution (V_T) as previously described (Hammers et al., 2007b).

Resolution recovery with SFS-RR

The Hammers^{mith} atlases, atlases of the human brain generated from manual definition of 83 anatomical structures for 30 normal subjects (Gousias et al., 2008; Hammers et al., 2003), were used to inform the resolution recovery process. An individualized anatomical atlas was prepared in three steps. First, each participant's MR image was tissue-class segmented using SPM5 according to the Unified Segmentation method (Ashburner and Friston, 2005). The grey matter component was then thresholded at 50% probability using Analyze AVW 8.1. Secondly, an individualized Hammers^{mith} atlas was created by 30 high-dimensional registrations between the MRIs underlying the 30 individual atlases and the target MRI, propagation of the associated atlases, and decision fusion in the target MRI space (Multi-Atlas Propagation with Enhanced Registration, MAPER (Heckemann et al., 2010)). In the third step, the outputs of the first and second steps were multiplied (Analyze AVW 8.1) to yield an individualized, anatomical atlas in the participant's MRI space, which was subsequently co-registered to his/her corresponding weighted summation (PET) images using SPM5 (Statistical Parametric Mapping software (SPM5; Wellcome Trust Centre for Neuroimaging, UCL, London, UK)).

Using MATLAB 7.4 (The MathWorks Inc., Natick, MA, USA) and the SFS-RR PVE correction method was applied in batch to the eight TLE datasets, and all eleven control datasets. The first step of SFS-RR (Fig. 1) is the decomposition of the PET (V_T) image and corresponding anatomical (in this case, MRI) image into multiple resolutions by a discrete wavelet transform (WT) (multi-resolution analysis; MRA; (Mallat, 1989; Turkheimer et al., 1999)). The process outlined above yields discrete wavelet coefficients, which provide an index of how similar each constituent wavelet is compared to a pre-defined analyzing wavelet (MathWorks, 1996). The second stage of SFS-RR involves replacement of the high-frequency wavelet coefficients of the PET image with those of the corresponding individualized, anatomical brain atlas (anatomical image). In the final stage, the resolution-recovered PET image is generated by application of the inverse of the wavelet transform.

Despite evidence that multi-atlas propagation with decision fusion in general (Gousias et al., 2008) and MAPER in particular are able to label atrophic hippocampi correctly (Heckemann et al., 2011), we wished to exclude the possibility that the results were biased by sub-optimal automated identification of sclerotic hippocampi. Therefore, SFS-RR was also separately applied using individualized Hammers^{mith} atlases after the incorporation of manual delineation of each subject's hippocampi into the MAPER-derived atlas according to a previously described protocol (Niemann et al., 2000), but extending more posteriorly, by a single operator (MF).

All transformations between PET and MRI spaces were performed using the corresponding weighted summation images (0–90 min data) in SPM5.

Analysis of recovered PET data

Analysis of PET data was by region-of-interest (ROI) approach, in regions implicated in the pathophysiology of temporal lobe epilepsy and/or informed by the prior voxel-by-voxel study without PVE correction (Hammers et al., 2007a,b). ROIs were the hippocampi, parahippocampal

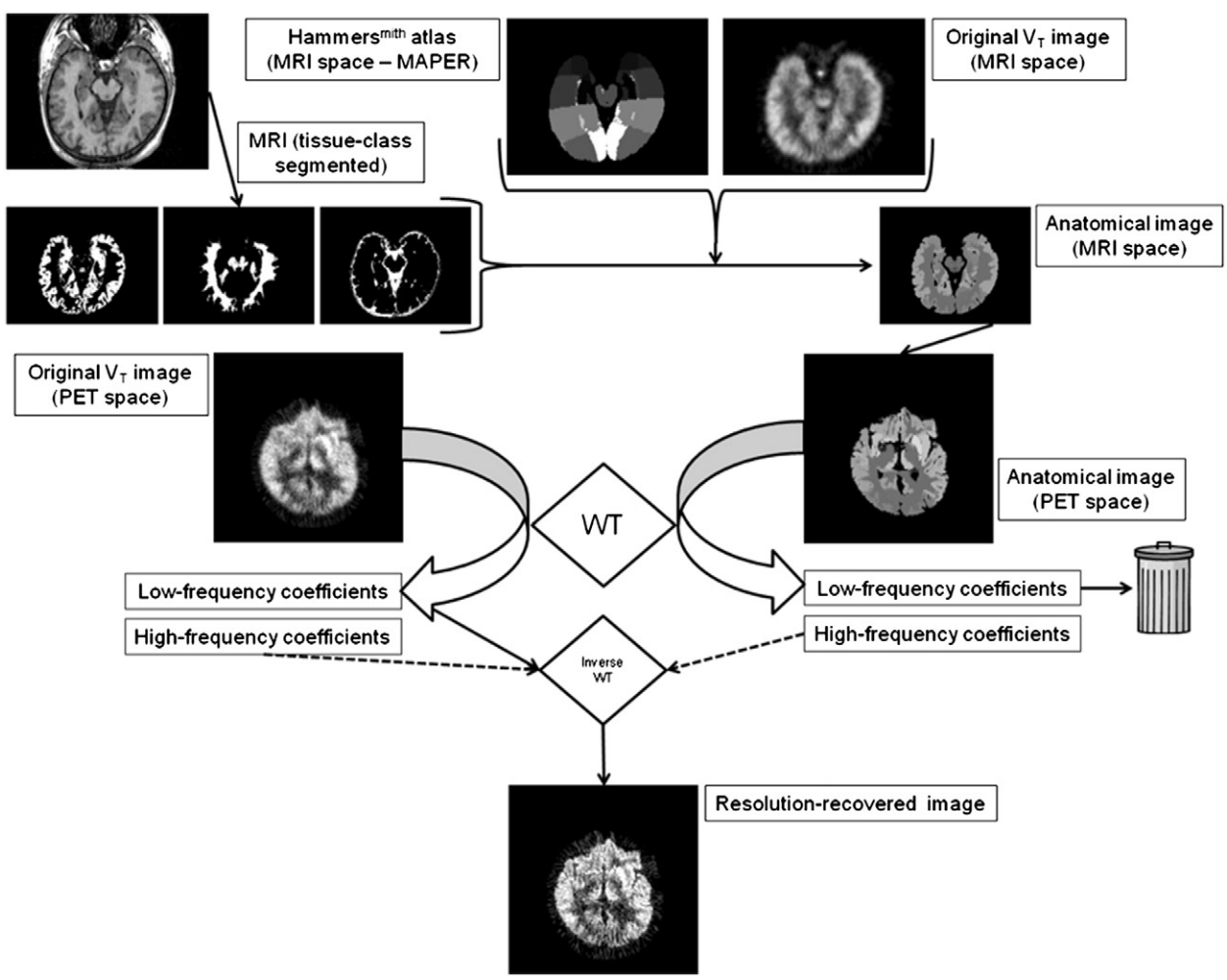

Fig. 1. Schematic diagram illustrating SFS-RR WT-discrete wavelet transform. Please refer to the Resolution recovery with SFS-RR section text for description.

gyri, amygdalae, fusiform gyri, lateral temporal poles, and sub-genual anterior cingulate gyri.

The ROI labels were left–right reversed after sampling for participants with a presumed right-sided epileptogenic focus, so that the focus was on the same side (left) in all eight participants with TLE. The [^{11}C]DPN V_T images of five of the healthy controls, selected at random using Random Sequence Generator(www.random.org), were also reversed. The VT images were then sampled via 'tac-test' (in-house software) using ROIs (object maps) created from the grey matter thresholded individual atlases.

As inter-subject variability in global V_T was considerable and differed between participant groups (16% controls group, 9% TLE group; see also Table 1), the average V_T values within each ROI were scaled relative to the global V_T according to the formula:

$$\text{Fractional ROI } V_T = \frac{\text{ROI } V_T}{\text{global } V_T}. \quad (1)$$

Statistical analyses

Statistical analysis was performed using SPSS for (Microsoft) Windows version 16.0 (SPSS Inc., IBM Corporation, Somers, New York, USA). For all analyses, the threshold of significance was set at $p < 0.05$. Correction for multiple comparisons was made using the Bonferroni method, except where stated otherwise.

Global [^{11}C]DPN V_T

Global [^{11}C]DPN V_T values were computed as follows: the overall mean over the entire matrix was thresholded at 1/8 of its value to create a brain mask; the mean over the entire matrix within this mask was then computed, using a MATLAB function derived in-house from the SPM default global value calculation.

Global [^{11}C]DPN V_T was compared between test (1st) and re-test (2nd) control scans using the non-parametric Wilcoxon signed-rank test. The influence of gender on global [^{11}C]DPN V_T was assessed by the non-parametric Mann–Whitney test (male *versus* female controls' mean values). The effect of spontaneous seizures on global [^{11}C]DPN V_T was assessed by the Wilcoxon signed-rank test (post-ictal *versus* interictal) and separately by the Mann–Whitney test (post-ictal *versus* controls' mean; interictal *versus* controls' mean).

The influence of hippocampal sclerosis on global [^{11}C]DPN V_T was assessed by Wilcoxon signed-rank tests (post-ictal-HS *versus* interictal-HS; post-ictal-MRI-normal *versus* interictal-MRI-normal) and Mann–Whitney tests (interictal-HS *versus* controls' mean; interictal-MRI-normal *versus* controls' mean).

The mean of the global [^{11}C]DPN V_T over test and re-test scans was computed for the controls group. This data was used to quantify the relationship between age and global [^{11}C]DPN V_T by Spearman's rho coefficient.

Regional [^{11}C]DPN V_T

The relationship between hippocampal [^{11}C]DPN V_T calculated using manually-delineated and MAPER-derived hippocampi was interrogated using Spearman's rho statistic. The same correlation was performed for the parahippocampal gyri (which were not manually delineated), to check the influence of manual hippocampal delineation on quantification of the nearby regions of interest. The delineation methods were also compared using a Tukey mean–difference plot.

The variability of test–re-test [^{11}C]DPN V_T was assessed for each ROI using the Wilcoxon signed-rank test. The relationships between age and [^{11}C]DPN V_T within each ROI (using the mean over left and right homologues) were assessed with Spearman's rho coefficient.

Table 1
Effect of SFS-RR on regional and global [^{11}C]DPN V_T data was generated using MAPER-derived ROIs.

(Region-of-interest)	Group	Hippocampi	[^{11}C]DPN V_T uncorrected (mean; s.d.)	[^{11}C]DPN V_T post-SFS-RR (mean; s.d.)	% change in [^{11}C]DPN V_T with SFS-RR (mean; s.d.)
Hippocampus	TLE	Sclerotic	13.1 (1.0)	13.5 (1.0)	3.3 (5.3)
		MRI-normal	13.4 (1.9)	14.0 (2.0)	4.2 (4.0)
		(Combined)	13.7 (1.8)	14.3 (1.8)	3.9 (4.6)
	Controls	MRI-normal	13.9 (2.3)	14.4 (2.5)	4.0 (1.3)
Parahippocampal gyrus	TLE	Sclerotic	13.4 (1.2)	14.6 (1.1)	9.2 (8.9)
		MRI-normal	13.8 (2.0)	14.9 (2.0)	7.8 (4.3)
		(Combined)	13.7 (1.7)	14.8 (1.7)	8.4 (6.3)
	Controls	MRI-normal	13.6 (2.5)	14.5 (2.7)	6.5 (1.3)
Amygdala	TLE	Sclerotic	16.0 (1.2)	17.8 (1.4)	11.6 (1.6)
		MRI-normal	17.0 (2.1)	18.8 (2.3)	10.8 (1.0)
		(Combined)	16.6 (1.9)	18.4 (2.1)	11.1 (1.3)
	Controls	MRI-normal	16.5 (2.9)	18.3 (3.1)	11.3 (2.2)
Fusiform gyrus	TLE	Sclerotic	16.0 (1.2)	16.9 (1.5)	5.9 (1.6)
		MRI-normal	16.0 (2.2)	17.0 (2.4)	6.2 (1.3)
		(Combined)	16.0 (1.9)	17.0 (2.1)	6.1 (1.4)
	Controls	MRI-normal	15.2 (2.7)	16.0 (2.8)	5.4 (1.4)
Lateral temporal pole	TLE	Sclerotic	15.9 (1.1)	17.4 (1.2)	9.6 (2.1)
		MRI-normal	16.5 (1.9)	18.2 (2.2)	10.1 (2.3)
		(Combined)	16.3 (1.6)	17.9 (1.9)	9.9 (2.2)
	Controls	MRI-normal	15.4 (3.2)	16.7 (3.6)	8.3 (2.5)
Anterior cingulate gyrus	TLE	Sclerotic	19.1 (0.6)	20.3 (0.8)	6.0 (1.3)
		MRI-normal	19.2 (1.7)	20.6 (1.9)	7.3 (1.7)
		(Combined)	19.1 (1.4)	20.5 (1.6)	6.8 (1.8)
	Controls	MRI-normal	18.6 (3.5)	19.9 (3.9)	6.3 (3.1)
Global	TLE	Sclerotic	10.4 (0.4)	11.3 (0.4)	8.3 (1.3)
		MRI-normal	10.8 (1.2)	12.2 (1.3)	12.9 (2.4)
		(Combined)	10.6 (0.8)	11.6 (1.0)	10.0 (2.9)
	Controls	MRI-normal	10.6 (1.7)	11.7 (1.9)	10.3 (3.5)

The effect of spontaneous seizures on [^{11}C]DPN V_T within each ROI was assessed as described above for the global [^{11}C]DPN V_T analysis. As no significant difference in [^{11}C]DPN V_T was evidenced across test and re-test data (see 'Results'), the mean V_T over both scans was computed for each ROI, for each participant, to inform comparisons with the interictal and post-ictal data. Ipsi- and contralateral [^{11}C]DPN V_T within each ROI was compared using the Wilcoxon signed-rank test. The influence of hippocampal sclerosis and gender on regional [^{11}C]DPN V_T, were also assessed as described above.

Correction for multiple comparisons was not performed for the main comparisons, as we had strong *a priori* hypotheses that an interictal decrease would be evident in sclerotic hippocampi, and that post-ictal increases would be evident in the ipsilateral temporal lobes of participants with TLE.

Results

An example of parametric [^{11}C]DPN V_T images before and after application of SFS-RR is provided in Fig. 2.

Effect of SFS-RR on hippocampal and global [^{11}C]DPN V_T

Global V_T values in the recovered images were increased by 10.0% (s.d. 2.9%) for participants with TLE, and 10.3% (s.d. 3.5%) for healthy controls, relative to the original uncorrected images (see Table 1).

Small increases in V_T were seen in the hippocampi ((4.2%, s.d. 4.0% in TLE with normal MRI; 4.0%, s.d. 1.3% in controls), 3.3%, s.d. 5.3% in sclerotic hippocampi).

All the global and regional [^{11}C]DPN V_T data presented subsequently are those after the application of SFS-RR.

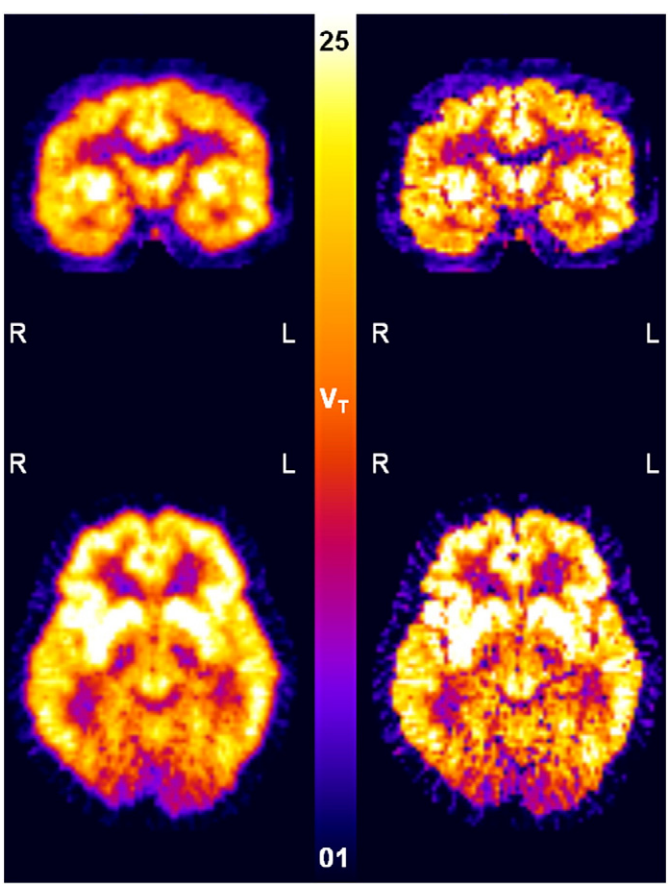

Fig. 2. Parametric V_T images pre- and post-SFS-RR.

Effect of spontaneous seizures and other variables on global [^{11}C]DPN V_T

There were no significant differences in global [^{11}C]DPN V_T between post-ictal, interictal, and control scans. There were also no significant differences in global [^{11}C]DPN V_T between test and re-test scans; between genders; or between participants whose TLE was associated with HS, participants with TLE associated with normal MRI, and controls.

There was no significant correlation between age and global [^{11}C]DPN V_T for the control group.

These findings indicated that epileptic seizures, epilepsy, gender, the presence of hippocampal sclerosis, and age did not significantly influence global [^{11}C]DPN V_T.

Effect of manual delineation versus MAPER on hippocampal [^{11}C]DPN V_T

Examples of regions of interest derived by MAPER and manual delineation of the hippocampi for a representative TLE group participant are provided in Fig. 3.

Quantification of [^{11}C]DPN V_T in manually-delineated hippocampi yielded very similar data to those obtained from hippocampi defined using MAPER (Table 2; Spearman's rho 0.948, $p < 0.001$; Fig. 4), despite differences in the volume of the structure. [^{11}C]DPN V_T was slightly reduced in the contralateral hippocampi of those with TLE, with manual delineation.

Manual delineation of hippocampi also had very little effect on quantification of V_T in the nearby parahippocampal gyri (Spearman's rho 0.983, $p < 0.001$), or on the global V_T. Therefore, all other regional data presented in this manuscript were obtained using the MAPER-derived ROIs.

Effect of test-re-test on regional [^{11}C]DPN V_T in controls

There were no significant differences in [^{11}C]DPN V_T between test and re-test conditions for any of the regions of interest in controls, indicating the test-re-test variability was low (see Table 3). The mean V_T over both scans was computed for each ROI, for each control, to inform comparisons with the interictal and post-ictal data.

Correlations between regional [^{11}C]DPN V_T and age

There were no significant correlations between age and [^{11}C]DPN V_T for any of the regions of interest.

Effect of spontaneous seizures and hippocampal sclerosis on regional [^{11}C]DPN V_T

After spontaneous seizures compared to both the interictal state and controls, there was a significant increase in [^{11}C]DPN V_T in the parahippocampal gyrus ($p = 0.012$ *versus* interictal; $p = 0.032$ *versus* controls; Table 3) ipsilateral to the electroclinical focus. This was not evident in the data prior to SFS-RR. Ipsilateral post-ictal V_T increases were also observed in the fusiform gyrus ($p = 0.012$; $p = 0.013$) and the lateral temporal pole (*versus* interictal only; $p = 0.036$), after SFS-RR. These latter two increases were also evident in the uncorrected data, *i.e.* prior to SFS-RR.

There was no significant difference in [^{11}C]DPN V_T between post-ictal, interictal, and control scans in the ipsilateral hippocampus, amygdala, and sub-genual anterior cingulate gyrus. In a post-hoc analysis (Mann–Whitney test), the magnitude of the post-ictal–interictal change in ipsilateral hippocampal [^{11}C]DPN V_T was greater for the TLE-MRI-normal group than for the TLE-HS group ($p = 0.025$) and control group ($p = 0.036$).

After spontaneous seizures compared to the interictal state and controls, there was a small increase in [^{11}C]DPN V_T in the fusiform gyrus ($p = 0.017$ *versus* interictal; $p = 0.012$ *versus* controls) contralateral to the electroclinical focus. The post-ictal [^{11}C]DPN V_T in the

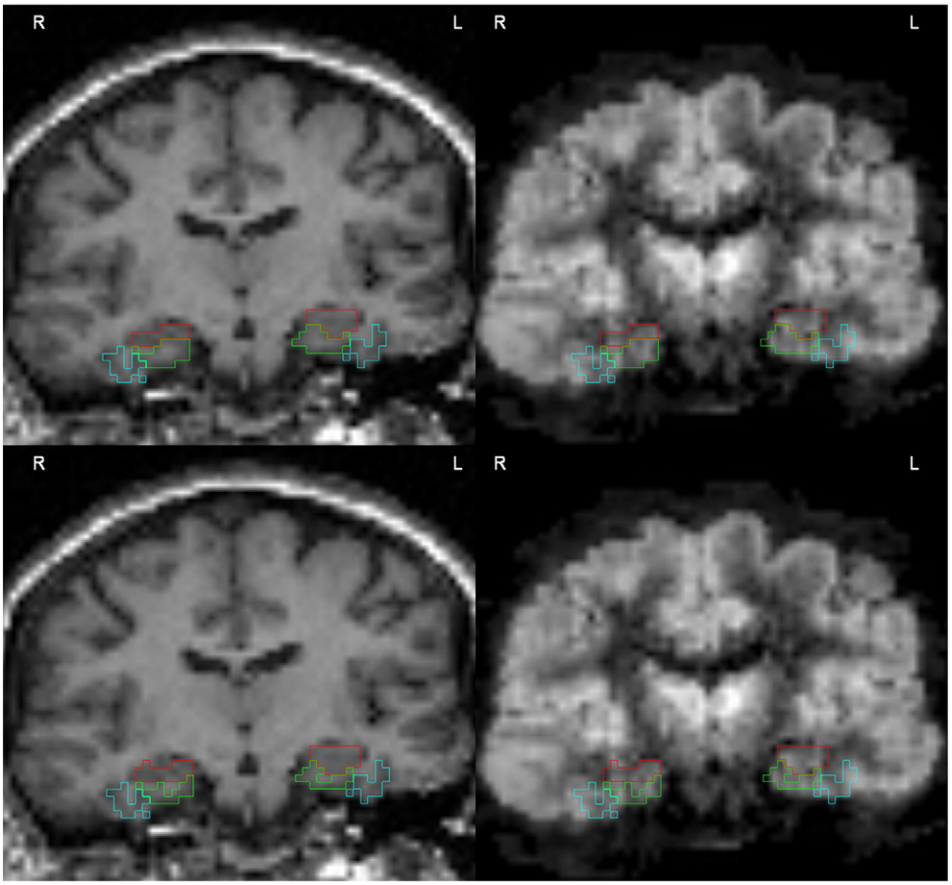

Fig. 3. Examples of regions of interest derived by MAPER (top row) and manual (bottom row) delineation for TLE group co-registered MR images (left) and [^{11}C]DPN V_T images (right; post-SFS-RR) are shown in radiological orientation. The hippocampi are delineated in red, the parahippocampal gyri in green, and the fusiform gyri in cyan. L — left; R — right.

contralateral temporal pole did not differ significantly from the interictal [^{11}C]DPN V_T in the same region, but was significantly greater than that seen in controls ($p = 0.012$).

There was no significant difference in [^{11}C]DPN V_T between post-ictal, interictal, and control scans within any of the other ROI homologues contralateral to the electroclinical focus.

There were no significant post-ictal decreases in [^{11}C]DPN V_T in any region of interest, when compared against the interictal state or controls.

[^{11}C]DPN V_T was significantly greater in the contralateral lateral temporal pole than in the ipsilateral temporal pole, in the interictal state only ($p = 0.012$). There were no other significant differences between ipsi- and contralateral [^{11}C]DPN V_T for any ROI, in either the post-ictal or interictal state.

Discussion

We have detected a post-ictal increase in [^{11}C]diprenorphine binding in the parahippocampal gyri in refractory TLE, which was not evident before denoising and PVE correction.

We were able to confirm previously reported increases in (scaled) opioid receptor availability of approximately 8% in the ipsilateral anterior temporal lobe following spontaneous seizures. After denoising and application of SFS-RR, the magnitude of the post-ictal increases

Table 2
Effect of manual delineation *versus* MAPER on hippocampal [^{11}C]DPN V_T (post SFS-RR).

(Region of interest)	Segmentation	Group	Lateralisation	Volume mm^3 mean (s.d.)	V_T mean (s.d.)
Hippocampus	MAPER	TLE	Ipsilateral	1782.0 (620.2)	14.1 (1.5)
		TLE	Contralateral	2190.0 (161.0)	14.4 (2.0)
		Controls	Left and right	2220.5 (314.9)	14.4 (2.4)
	Manual	TLE	Ipsilateral	2420.1 (732.0)	14.1 (1.5)
		TLE	Contralateral	3117.5 (779.8)	14.1 (2.0)
		Controls	Left and right	2706.5 (473.2)	14.4 (2.3)
Parahippocampal gyri	MAPER	TLE	Ipsilateral	3333.0 (776.6)	14.8 (1.5)
		TLE	Contralateral	3780.0 (336.6)	14.8 (1.9)
		Controls	Left and right	3954.6 (550.3)	14.5 (2.7)
	Manual	TLE	Ipsilateral	3015.1 (786.0)	14.9 (1.6)
		TLE	Contralateral	3333.2 (386.8)	15.0 (2.0)
		Controls	Left and right	3465.5 (406.0)	14.7 (2.7)
Global	MAPER	TLE	n/a	n/a	11.6 (1.0)
		Controls	n/a	n/a	11.7 (1.9)
	Manual	TLE	n/a	n/a	11.6 (1.0)
		Controls	n/a	n/a	11.8 (1.9)

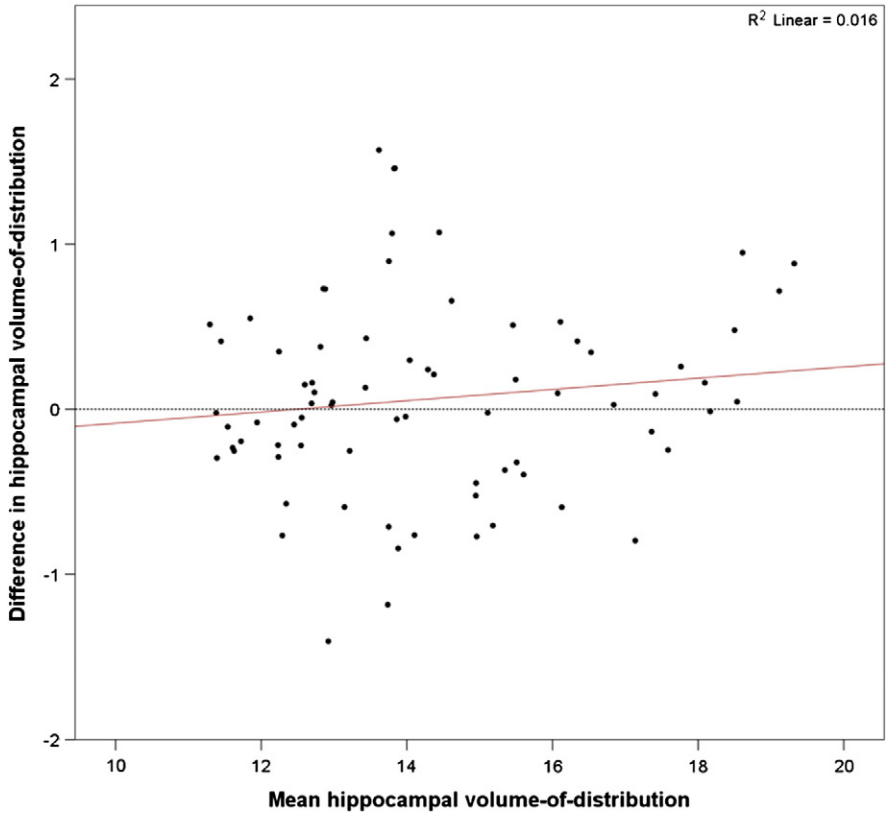

Fig. 4. Comparison of [^{11}C]DPN V_T extracted from MAPER-derived and manually-delineated hippocampi Tukey mean-difference plot (also known as Bland–Altman plot); a very slight bias (~1%) towards overestimation is seen with MAPER for hippocampi with high V_T.

Table 3
Effect of spontaneous seizures on regional [^{11}C]DPN V_T (post-SFS-RR) Data was generated using MAPER-derived ROIs.

(Region-of-interest)	Group	Lateralisation	$V_{T\text{-}ROI}$:$V_{T\text{-}global}$ mean (s.d.) Scan 1 (controls)/ post-ictal scan (TLE group)	$V_{T\text{-}ROI}$:$V_{T\text{-}global}$ mean (s.d.) Scan 2 (controls)/ interictal scan (TLE group)
Hippocampus	TLE	Ipsilateral	1.23 (0.11)	1.19 (0.09)
		Contralateral	1.25 (0.12)	1.22 (0.12)
	Controls	Left	**1.22 (0.11)**	**1.22 (0.11)**
		Right	**1.24 (0.09)**	**1.24 (0.11)**
Parahippocampal gyrus	TLE	Ipsilateral	1.32 (0.08)*,#	1.23 (0.10)
		Contralateral	1.28 (0.11)	1.25 (0.07)
	Controls	Left	**1.24 (0.09)**	**1.23 (0.09)**
		Right	**1.24 (0.09)**	**1.22 (0.11)**
Amygdala	TLE	Ipsilateral	1.62 (0.13)	1.53 (0.16)
		Contralateral	1.61 (0.13)	1.59 (0.09)
	Controls	Left	**1.56 (0.12)**	**1.58 (0.15)**
		Right	**1.54 (0.12)**	**1.57 (0.13)**
Fusiform gyrus	TLE	Ipsilateral	1.52 (0.13)*,#	1.38 (0.15)
		Contralateral	1.51 (0.10)*,#	1.43 (0.11)
	Controls	Left	**1.36 (0.11)**	**1.35 (0.13)**
		Right	**1.37 (0.11)**	**1.37 (0.12)**
Lateral temporal pole	TLE	Ipsilateral	1.59 (0.13)*	1.43 (0.09)
		Contralateral	1.62 (0.12)#	1.53 (0.03)
	Controls	Left	**1.43 (0.16)**	**1.41 (0.22)**
		Right	**1.42 (0.17)**	**1.42 (0.21)**
Anterior cingulate gyrus	TLE	Ipsilateral	1.75 (0.10)	1.75 (0.11)
		Contralateral	1.78 (0.11)	1.76 (0.10)
	Controls	Left	**1.68 (0.13)**	**1.70 (0.10)**
		Right	**1.68 (0.08)**	**1.67 (0.11)**
Global V_T	TLE	n/a	11.44 (1.14)	11.83 (0.87)
	Controls	n/a	**11.92 (1.90)**	**11.58 (2.02)**

* $p < 0.05$ *versus* interictal.
\# $p < 0.05$ *versus* controls.

was increased to approximately 12–16% (see Table 3). Smaller increases were also identified in the contralateral fusiform gyri and temporal pole. Despite full quantification including arterial input functions and PVE correction, the post-ictal increases were only observed when differences in global mean were accounted for, in a manner analogous to SPM analyses.

The denoising, multi-atlas segmentation, and RR techniques employed here expose the implication of several temporal lobe regions: parahippocampal gyrus, fusiform gyrus, and lateral temporal pole. Correction for multiple comparisons was not performed as the analyses were not exploratory (a hypothesis was defined *a priori*) and the [^{11}C]DPN V_T in medial temporal lobe regions-of-interest are correlated (Turkheimer et al., 2004). The novel finding of post-ictal increases in the parahippocampal gyrus is notable, as previously only Rocha et al. (Rocha et al., 2007) had been able to identify altered opioid receptor binding in this region.

Interestingly, we found that correction for global V_T was necessary for the demonstration of focal post-ictal increases in [^{11}C]DPN V_T using a regions of interest approach. Across participants and test and re-test scans, we noted a coefficient of variation in global V_T of approximately 16% for controls. In medicated participants such as those in our TLE group, it is conceivable that differing drug regimens could variably influence global V_T. Correction for global uptake is routine in voxel-based analyses such as tests based on the comparison of parametric images. Our findings suggest that it should also be considered for ROI analyses to facilitate the identification of small but potentially meaningful alterations in radioligand uptake/distribution.

We do not expect [^{11}C]diprenorphine PET to find routine clinical application, as it requires an on-site cyclotron as well as arterial blood sampling. However, accurate quantification of distribution without an arterial plasma input function might be possible using rank-shaping regularization of exponential spectral analyses (RS-ESA; (Turkheimer et al.,

2003, 2012)); additional novel approaches might become available in the future. Alternatively, reference regions do exist for certain subtype-specific opioid peptide receptor radioligands, such as [^{11}C]carfentanil.

Limitations

The use of voxel-based techniques in our earlier analyses (Hammers et al., 2007a) implies spatial transformations of the original imaging data and could arguably have induced artifacts. It is reassuring that post-ictal [^{11}C]DPN V_T increases in the ipsilateral fusiform gyrus and lateral temporal pole could be confirmed with the present technique in native space. Whilst this is the first application of SFS-RR to [^{11}C] diprenorphine data, detailed evaluation in 15 simulated [^{11}C]raclopride data sets showed consistent resolution recovery that was influenced by the quality of the structural atlas only (Shidahara et al., 2012).

The major limitation of our work is the small sample size, due to the difficulties in recruiting for and performing post-ictal quantitative PET studies (Hammers et al., 2007a). The TLE group also includes participants with and without HS. In addition, and as highlighted in the initial study (Hammers et al., 2007a), the exact duration of the interval between last seizure and PET scan was not quantified with certainty, as electroencephalography–telemetry was not available.

Another limitation is that [^{11}C]DPN has quite a low volume-of-distribution in the hippocampus, when compared with that of surrounding regions; hence, the ability to reliably detect significant alterations in binding in this region may be reduced.

In this study, SFS-RR was applied to parametric V_T images. Theoretically, it would be preferable to apply the PVC methodology to the individual (dynamic image) frames. However, this is not feasible because of the very low signal-to-noise ratio of the individual frames, and in particular of those acquired just after radioligand injection and of the late frames. The approach has been attempted (Reilhac et al., 2011), but it has seldom, if ever, been used to analyze clinical datasets. Shidahara et al. (2012) applied SFS-RR to two simulated, dynamic [^{11}C]raclopride datasets; whilst recovery was impressive, considerable noise enhancement was evident.

Conclusions

Our findings provide further direct human *in vivo* evidence for interictal and post-ictal alterations of opioid peptide receptor availability in TLE. We demonstrated that denoising, resolution recovery and precise anatomical segmentation can extract valuable information from PET studies that would be missed with conventional post-processing procedures. Correction for global uptake can facilitate the identification of small but potentially significant alterations in radioligand distribution with regions of interest analyses.

Acknowledgments

We thank all who volunteered to participate in this study as a subject.

This study was supported by the Medical Research Council Clinical Sciences Centre (G9901497; G108/585). Authors affiliated with [a] are grateful for support from the NIHR Biomedical Research Centre funding scheme.

CJM was supported by a Medical Research Council Doctoral Training Account (3 + 1) studentship that was awarded by Imperial College London.

RAH was supported by a research grant from the Dunhill Medical Trust.

JSD and MJK are supported by the Epilepsy Society, UCL and UCL Hospitals. JD has received fees for organizing symposia for UCB Pharma, Eisai and GE Healthcare.

FET was supported by the MRC PET Methodology Programme Grant (G1100809/1). AH was supported by an MRC Clinician Scientist Fellowship (G108/585) and the Neurodis Foundation.

References

Ashburner, J., Friston, K.J., 2005. Unified segmentation. Neuroimage 26, 839–851.

Aston, J.A., Cunningham, V.J., Asselin, M.C., Hammers, A., Evans, A.C., Gunn, R.N., 2002. Positron emission tomography partial volume correction: estimation and algorithms. J. Cereb. Blood Flow Metab. 22, 1019–1034.

Bartenstein, P.A., Duncan, J.S., Prevett, M.C., Cunningham, V.J., Fish, D.R., Jones, A.K., Luthra, S.K., Sawle, G.V., Brooks, D.J., 1993. Investigation of the opioid system in absence seizures with positron emission tomography. J. Neurol. Neurosurg. Psychiatry 56, 1295–1302.

Bernasconi, N., Bernasconi, A., Caramanos, Z., Antel, S.B., Andermann, F., Arnold, D.L., 2003. Mesial temporal damage in temporal lobe epilepsy: a volumetric MRI study of the hippocampus, amygdala and parahippocampal region. Brain 126, 462–469.

Chaturvedi, K., Christoffers, K.H., Singh, K., Howells, R.D., 2000. Structure and regulation of opioid receptors. Biopolymers 55, 334–346.

Cuellar-Herrera, M., Velasco, A.L., Velasco, F., Chavez, L., Orozco-Suarez, S., Armagan, G., Turunc, E., Bojnik, E., Yalcin, A., Benyhe, S., Borsodi, A., Alonso-Vanegas, M., Rocha, L., 2012. Mu opioid receptor mRNA expression, binding, and functional coupling to G-proteins in human epileptic hippocampus. Hippocampus 22, 122–127.

Cunningham, V.J., Jones, T., 1993. Spectral analysis of dynamic PET studies. J. Cereb. Blood Flow Metab. 13, 15–23.

Dhawan, B.N., Cesselin, F., Raghubir, R., Reisine, T., Bradley, P.B., Portoghese, P.S., Hamon, M., 1996. International Union of Pharmacology. XII. Classification of opioid receptors. Pharmacol. Rev. 48, 567–592.

Engel Jr., J., Ackermann, R., Caldecott-Hazard, S., Kuhl, D., 1981. Epileptic activation of antagonistic systems may explain paradoxical features of experimental and human epilepsy: a review and hypothesis. Raven Press, New York.

Frost, J.J., Mayberg, H.S., Fisher, R.S., Douglass, K.H., Dannals, R.F., Links, J.M., Wilson, A.A., Ravert, H.T., Rosenbaum, A.E., Snyder, S.H., et al., 1988. Mu-opiate receptors measured by positron emission tomography are increased in temporal lobe epilepsy. Ann. Neurol. 23, 231–237.

Gousias, I.S., Rueckert, D., Heckemann, R.A., Dyet, L.E., Boardman, J.P., Edwards, A.D., Hammers, A., 2008. Automatic segmentation of brain MRIs of 2-year-olds into 83 regions of interest. Neuroimage 40, 672–684.

Hammers, A., Lingford-Hughes, A., 2006. Opioid imaging. Neuroimaging Clin. N. Am. 16, 529–552 (vii).

Hammers, A., Allom, R., Koepp, M.J., Free, S.L., Myers, R., Lemieux, L., Mitchell, T.N., Brooks, D.J., Duncan, J.S., 2003. Three-dimensional maximum probability atlas of the human brain, with particular reference to the temporal lobe. Hum. Brain Mapp. 19, 224–247.

Hammers, A., Asselin, M.C., Hinz, R., Kitchen, I., Brooks, D.J., Duncan, J.S., Koepp, M.J., 2007a. Upregulation of opioid receptor binding following spontaneous epileptic seizures. Brain 130, 1009–1016.

Hammers, A., Asselin, M.C., Turkheimer, F.E., Hinz, R., Osman, S., Hotton, G., Brooks, D.J., Duncan, J.S., Koepp, M.J., 2007b. Balancing bias, reliability, noise properties and the need for parametric maps in quantitative ligand PET: [^{11}C]diprenorphine test-retest data. Neuroimage 38, 82–94.

Heckemann, R.A., Keihaninejad, S., Aljabar, P., Rueckert, D., Hajnal, J.V., Hammers, A., 2010. Improving intersubject image registration using tissue-class information benefits robustness and accuracy of multi-atlas based anatomical segmentation. Neuroimage 51, 221–227.

Heckemann, R.A., Keihaninejad, S., Aljabar, P., Gray, K.R., Nielsen, C., Rueckert, D., Hajnal, J.V., Hammers, A., 2011. Automatic morphometry in Alzheimer's disease and mild cognitive impairment. Neuroimage 56, 2024–2037.

Hoffman, E.J., Huang, S.C., Phelps, M.E., 1979. Quantitation in positron emission computed tomography: 1. Effect of object size. J. Comput. Assist. Tomogr. 3, 299–308.

ILAE Commission on Neurosurgery of Epilepsy, 2004. Mesial temporal lobe epilepsy with hippocampal sclerosis. Epilepsia 45, 695–714.

Koepp, M.J., Duncan, J.S., 2000. PET: opiate neuroreceptor mapping. Adv. Neurol. 83, 145–156.

Koepp, M.J., Richardson, M.P., Brooks, D.J., Duncan, J.S., 1998. Focal cortical release of endogenous opioids during reading-induced seizures. Lancet 352, 952–955.

Loacker, S., Sayyah, M., Wittmann, W., Herzog, H., Schwarzer, C., 2007. Endogenous dynorphin in epileptogenesis and epilepsy: anticonvulsant net effect via kappa opioid receptors. Brain 130, 1017–1028.

Luthra, S.K., Osman, S., Turton, D.R., Vaja, J., Dowsett, K., Brady, F., 1993. An automated system based on solid phase extraction and HPLC for the routine determination in plasma of unchanged [^{11}C]-L-deprenyl; [^{11}C]diprenorphine; [^{11}C]raclopride; and [^{11}C]Schering 23390. J. Labelled Comp. Radiopharm. 32, 518–520.

Madar, I., Lesser, R.P., Krauss, G., Zubieta, J.K., Lever, J.R., Kinter, C.M., Ravert, H.T., Musachio, J.L., Mathews, W.B., Dannals, R.F., Frost, J.J., 1997. Imaging of delta- and mu-opioid receptors in temporal lobe epilepsy by positron emission tomography. Ann. Neurol. 41, 358–367.

Mallat, S.G., 1989. A theory for multiresolution signal decomposition: the wavelet representation. IEEE Trans. Pattern Anal. Mach. Intell. 11, 674–693.

MathWorks, I.T., 1996. Applications Using Wavelets with MATLAB and the Wavelet Toolbox. The MathWorks Inc.

Mayberg, H.S., Sadzot, B., Meltzer, C.C., Fisher, R.S., Lesser, R.P., Dannals, R.F., Lever, J.R., Wilson, A.A., Ravert, H.T., Wagner Jr., H.N., 1991. Quantification of mu and non-mu opiate receptors in temporal lobe epilepsy using positron emission tomography. Ann. Neurol. 30, 3–11.

Meltzer, C.C., Zubieta, J.K., Brandt, J., Tune, L.E., Mayberg, H.S., Frost, J.J., 1996. Regional hypometabolism in Alzheimer's disease as measured by positron emission tomography after correction for effects of partial volume averaging. Neurology 47, 454–461.

Niemann, K., Hammers, A., Coenen, V.A., Thron, A., Klosterkotter, J., 2000. Evidence of a smaller left hippocampus and left temporal horn in both patients with first episode schizophrenia and normal control subjects. Psychiatry Res. 99, 93–110.

Pirker, S., Gasser, E., Czech, T., Baumgartner, C., Schuh, E., Feucht, M., Novak, K., Zimprich, F., Sperk, G., 2009. Dynamic up-regulation of prodynorphin transcription in temporal lobe epilepsy. Hippocampus 19, 1051–1054.

Reilhac, A., Lehnert, W., Lin, J., Meikle, S.R., Gregoire, M.C., 2011. Iterative-based partial volume effects corrections with wavelet-based regularization for quantitative PET imaging. IEEE Nuclear Science Symp. and Medical Imaging Conf. IEEE, Valencia, pp. 3788–3791.

Rocha, L., Cuellar-Herrera, M., Velasco, M., Velasco, F., Velasco, A.L., Jimenez, F., Orozco-Suarez, S., Borsodi, A., 2007. Opioid receptor binding in parahippocampus of patients with temporal lobe epilepsy: its association with the antiepileptic effects of subacute electrical stimulation. Seizure 16, 645–652.

Satoh, M., Minami, M., 1995. Molecular pharmacology of the opioid receptors. Pharmacol. Ther. 68, 343–364.

Shidahara, M., Tsoumpas, C., Hammers, A., Boussion, N., Visvikis, D., Suhara, T., Kanno, I., Turkheimer, F.E., 2009. Functional and structural synergy for resolution recovery and partial volume correction in brain PET. Neuroimage 44, 340–348.

Shidahara, M., Tsoumpas, C., McGinnity, C.J., Kato, T., Tamura, H., Hammers, A., Watabe, H., Turkheimer, F.E., 2012. Wavelet-based resolution recovery using an anatomical prior provides quantitative recovery for human population phantom PET [^{11}C] raclopride data. Phys. Med. Biol. 57, 3107–3122.

Tortella, F.C., 1988. Endogenous opioid peptides and epilepsy: quieting the seizing brain? Trends Pharmacol. Sci. 9, 366–372.

Turkheimer, F.E., Brett, M., Visvikis, D., Cunningham, V., 1999. Multiresolution analysis of emission tomography images in the wavelet domain. J. Cereb. Blood Flow Metab. 19, 1189–1208.

Turkheimer, F.E., Hinz, R., Gunn, R.N., Aston, J.A., Gunn, S.R., Cunningham, V.J., 2003. Rank-shaping regularization of exponential spectral analysis for application to functional parametric mapping. Phys. Med. Biol. 48, 3819–3841.

Turkheimer, F.E., Aston, J.A., Cunningham, V.J., 2004. On the logic of hypothesis testing in functional imaging. Eur. J. Nucl. Med. Mol. Imaging 31, 725–732.

Turkheimer, F.E., Selvaraj, S., Hinz, R., Murthy, V., Bhagwagar, Z., Grasby, P., Howes, O., Rosso, L., Bose, S.K., 2012. Quantification of ligand PET studies using a reference region with a displaceable fraction: application to occupancy studies with [lsqb]^{11}C[rsqb]-DASB as an example. J. Cereb. Blood Flow Metab. 32, 70–80.

Yilmazer-Hanke, D.M.M., Wolf, H.K.M., Schramm, J.M., Elger, C.E.M., Wiestler, O.D.M., Blumcke, I.M., 2000. Subregional pathology of the amygdala complex and entorhinal region in surgical specimens from patients with pharmacoresistant temporal lobe epilepsy. J. Neuropathol. Exp. Neurol. 59, 907–920.